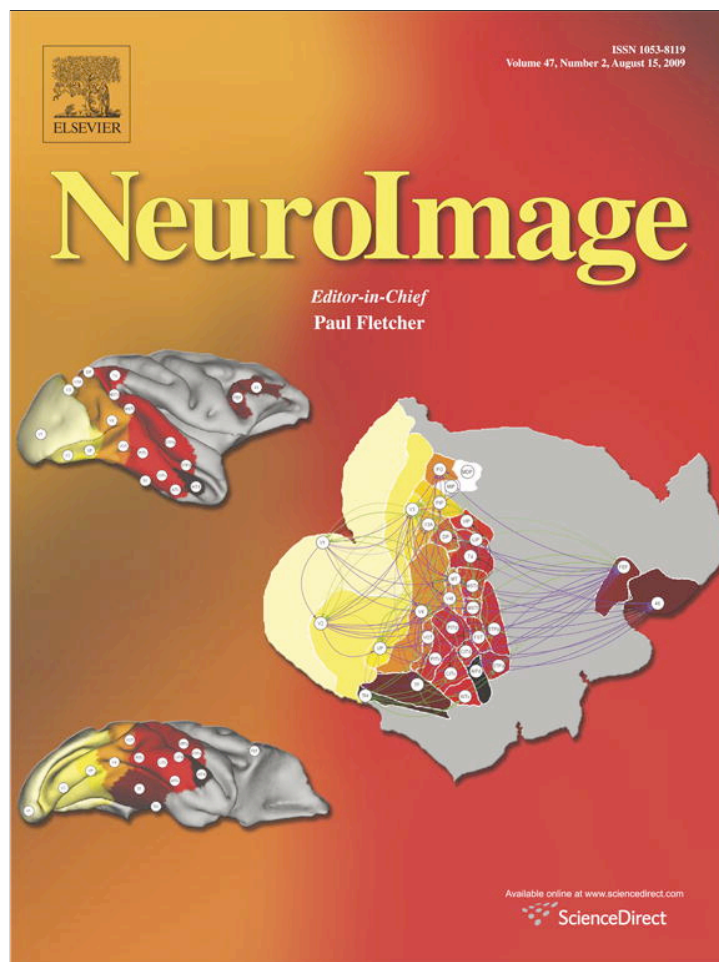


Provided for non-commercial research and education use.
Not for reproduction, distribution or commercial use.



This article appeared in a journal published by Elsevier. The attached copy is furnished to the author for internal non-commercial research and education use, including for instruction at the authors institution and sharing with colleagues.

Other uses, including reproduction and distribution, or selling or licensing copies, or posting to personal, institutional or third party websites are prohibited.

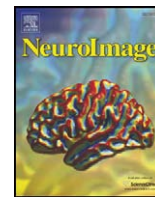
In most cases authors are permitted to post their version of the article (e.g. in Word or Tex form) to their personal website or institutional repository. Authors requiring further information regarding Elsevier's archiving and manuscript policies are encouraged to visit:

<http://www.elsevier.com/copyright>



Contents lists available at ScienceDirect

NeuroImage

journal homepage: www.elsevier.com/locate/ynimg

Single-trial reconstruction of finger-pinch forces from human motor-cortical activation measured by near-infrared spectroscopy (NIRS)

Isao Nambu^{a,b,*}, Rieko Osu^{a,c}, Masa-aki Sato^a, Soichi Ando^d, Mitsuo Kawato^{a,b}, Eiichi Naito^{a,c}

^a ATR Computational Neuroscience Laboratories, Kyoto, Japan

^b Graduate School of Information Science, Nara Institute of Science and Technology, Nara, Japan

^c National Institute of Information and Communications Technology, Kyoto, Japan

^d Graduate School of Sport Science, Osaka University of Health and Sport Sciences, Osaka, Japan

ARTICLE INFO

Article history:

Received 4 December 2008

Revised 10 March 2009

Accepted 9 April 2009

Available online 22 April 2009

ABSTRACT

Near-infrared spectroscopy (NIRS) has recently been used to measure human motor-cortical activation, enabling the classification of the content of a sensory-motor event such as whether the left or right hand was used. Here, we advance this NIRS application by demonstrating quantitative estimates of multiple sensory-motor events from single-trial NIRS signals. It is known that different degrees of sensory-motor activation are required to generate various hand/finger force levels. Thus, using a sparse linear regression method, we examined whether the temporal changes in different force levels could be reconstructed from NIRS signals. We measured the relative changes in oxyhemoglobin concentrations in the bilateral sensory-motor cortices while participants performed an isometric finger-pinch force production with their thumb and index finger by repeatedly exerting one of three target forces (25, 50, or 75% of the maximum voluntary contraction) for 12 s. To reconstruct the generated forces, we determined the regression parameters from the training datasets and applied these parameters to new test datasets to validate the parameters in the single-trial reconstruction. The temporal changes in the three different levels of generated forces, as well as the baseline resting state, could be reconstructed, even for the test datasets. The best reconstruction was achieved when using only the selected NIRS channels dominantly located in the contralateral sensory-motor cortex, and with a four second hemodynamic delay. These data demonstrate the potential for reconstructing different levels of external loads (forces) from those of the internal loads (activation) in the human brain using NIRS.

© 2009 Elsevier Inc. All rights reserved.

Introduction

Near-infrared spectroscopy (NIRS) is an emerging neuroimaging technique, which allows measurement of human brain activity while people perform a wide range of daily tasks (Villringer and Chance, 1997; Obrig and Villringer, 2003; Hoshi, 2003; Koizumi et al., 2003). Due to its practical advantages of portability, simplicity of use, freedom from electrical-noise, and lower sensitivity to body-motion artifacts, NIRS has also been used to investigate brain activity related to human motor control.

Although several NIRS studies have shown the importance of sensory-motor cortical regions in human motor control (Obrig et al., 1996; Watanabe et al., 1996; Miyai et al., 2001; Hatakenaka et al., 2007), as well established by other neuroimaging techniques such as functional magnetic resonance imaging (fMRI) and positron emission tomography (PET), the interpretation of NIRS data remains controversial (Boas et al., 2004). This is mainly because NIRS signals are

considered to contain background physiological signals such as cardiac pulsations, respiration, and blood pressure variations, which change with the task epoch (Obrig et al. 2000; Boas et al. 2004). Indeed, previous studies have suggested that NIRS signals may reflect changes in systemic signals that can be observed in brain areas which are probably not related to a task (Leung et al., 2003; Tachtsidis et al., 2008a,b). Thus, the conventional approach of averaging NIRS signals may be limited for purely identifying a task-related activation that essentially reflects its brain computation.

To examine whether brain activation is essentially related to neuronal computation in a motor task and necessary to perform that task, one possible approach is single-trial reconstruction where task-related variables (e.g., generated forces or muscular activity) are reconstructed or predicted from a selected set of brain activation. Evaluating the reconstruction accuracy increases the chance of identifying the essential set of brain activation for a motor task. However, even the most advanced NIRS application is still limited to the binary classification of a single sensory-motor event, e.g., whether the left or right hand was used when performing or imagining hand movements in a single trial (Coyle et al., 2004, 2007; Sitaram et al., 2007). In the present study, we advance the current level of NIRS

* Corresponding author. ATR Computational Neuroscience Laboratories, 2-2-2 Hikaridai, Seika, Soraku-gun, Kyoto, 619-0288, Japan. Fax: +81 774 95 1236.
E-mail addresses: isao-n@atr.jp (I. Nambu), enaito@atr.jp (E. Naito).

application by demonstrating the reconstruction of temporal changes in the dynamic aspects of multiple sensory-motor events from a NIRS signal, thus validating the use of a single-trial NIRS signal to quantitatively estimate a task-related variable.

In humans (Dettmers et al., 1995, 1996; Thickbroom et al., 1998; Dai et al., 2001; Cramer et al., 2002) and non-human primates (Evarts, 1968; Cheney and Fetz, 1980), it is well established that sensory-motor cortical regions, especially in the contralateral hemisphere, are involved in the generation of a hand/finger force, and that the neuronal activities of these regions correlate with the magnitude of the generated force. This fact, which was revealed by averaging multiple datasets/sessions, directly indicates that the magnitude of a generated force can be reconstructed from human sensory-motor cortical activation. Indeed, it has been demonstrated that it is possible to reconstruct the magnitude of a generated force and the level of muscular activity from neuronal activity in sensory-motor areas on single-trial basis (Carmena et al., 2003; Morrow and Miller, 2003; Ting et al., 2005, 2008; Koike et al., 2006). Furthermore, a recent non-invasive human study demonstrated reconstruction of individual muscular activity from blood oxygenation level-dependent (BOLD) signals (Ganesh et al., 2008). Thus, if the NIRS signal reflects local activation in sensory-motor cortical regions then quantitative changes in finger-pinch forces should be able to be reconstructed from the sensory-motor cortical activation, especially from those in the contralateral hemisphere. Furthermore, since the NIRS signal largely depends on relative changes in the regional cerebral blood flow in the cortical regions (Hoshi et al., 2001; Obrig and Villringer, 2002), then the best single-trial reconstruction are achieved when considering the physiological factor of its hemodynamics (hemodynamic delay).

In the present study, using NIRS we measured the oxyhemoglobin concentrations (oxy-Hb) in the bilateral sensory-motor cortices while participants generated three different levels of isometric finger-pinch forces with their thumb and index finger. To select the set of NIRS channels that contain task-relevant information for reconstruction, we used a sparse linear regression method (Sato et al., 2004b; Toda et al., 2007; Ting et al., 2005, 2008), which automatically determines the essential channels for linear regression. The reconstruction performance using this method was then compared with that of ordinary linear regression using all channels without channel selection, as well with only channels selected through a brute-force channel search.

Material and methods

Participants

Five right-handed healthy volunteers (four male and one female, 23 to 38 years of age) participated in this experiment. The ethical committee of the National Institute of Information and Communications Technology (NICT) approved the experiment, and all participants gave written informed consent. The experiment was performed in accordance with the latest version of the Declaration of Helsinki.

Protocol

The participants generated isometric finger-pinch forces with their thumb and index finger (Fig. 1a) using either the left- or right-hand for 12 s at 1 Hz, paced by a beep sound (Fig. 1b). The force was exerted on an acrylic board to which a force transducer was attached (PS-10KA; Kyowa Electronic Instruments, Chofu, Japan). Each force generation lasted for approximately 500 ms. Prior to the experiment, the force level of the maximal voluntary contraction (MVC) between the fingers was measured for each participant, and all participants were trained to exert target forces at three different levels, corresponding to 25%, 50%, and 75% of the MVC. The exerted force levels were continuously monitored by software (PowerLab; AD Instruments, Castle Hill, Australia) and displayed on a monitor as visual feedback. For the behavioral training, the participants repeated the task by viewing the feedback about their exerted force levels until they could successfully exert the target forces with their eyes closed. The experiments were then performed while the participants closed their eyes to avoid the concomitance of visual effects into the NIRS signals. During the experiment, an observer monitored the target forces, and when latter became markedly greater or smaller than the targets, a short verbal feedback was given.

In the experiment, ten sessions were assigned for each hand. Three participants conducted the task with both their left- and right-hands, and two participants completed the task with only the right hand. The left-hand experiments were cancelled according to the Declaration of Helsinki, as these two participants felt discomfort and pain generated by NIRS holders during the experiment. Overall, a total of eight datasets (hands) were obtained in the experiment. Each session consisted of six 12 s epochs with inter-epoch-intervals of 21 s. The

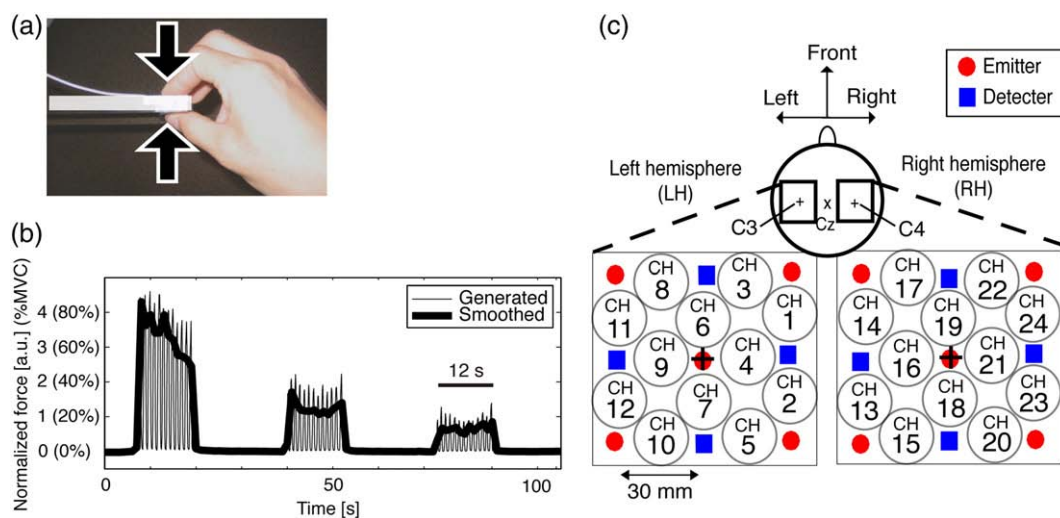


Fig. 1. Experimental procedure. (a) An isometric force production task using the right thumb and index finger. Force magnitudes were measured using a force transducer on an acrylic board. (b) Time-course of measured force. The force that was actually generated (thin line) was smoothed at 1 Hz (bold line). In one epoch, the 1 Hz force production was repeated for 12 s. (c) Channel locations in NIRS measurement. A channel (black number) was defined as an intermediate position between a light-emitter (red circle) and a light-detector (blue rectangle). The distance between the emitter and detector was 30 mm. The emitter in the center of each holder was located at C3 (left) and C4 (right), respectively, based on the International 10–20 System.

exerted forces were measured at a sampling rate of 1 kHz. In each session, the three force levels were repeated twice and their order was pseudo-randomized. The participants were informed of the force levels just before each trial was started.

NIRS measurements

We used a 24-channel NIRS system (ETG-100; Hitachi Medical Corporation, Tokyo, Japan) to measure the relative changes in oxy-Hb and deoxyhemoglobin (deoxy-Hb) concentrations at 780 nm and 830 nm wavelengths, respectively. The principles of this system have been previously described (Maki et al., 1995; Koizumi et al., 1999). A pair of NIRS holders, each of which contained 12 channels, was placed over the sensory-motor regions of the left and right hemispheres (Fig. 1c). The centers of these holders were located at positions C3 (left) and C4 (right) of the International 10–20 System, respectively. The NIRS signal was recorded at a sampling rate of 10 Hz.

Preprocessing

For the present analysis we only used oxy-Hb data as it reflects changes in regional cerebral blood flow better than deoxy-Hb (Hoshi et al., 2001), and because our NIRS system was not completely suitable for detecting deoxy-Hb changes due to the wavelengths (Sato et al., 2004a). For each session, the raw oxy-Hb data was averaged every second, and then these data were converted into a z-score that was normalized by its variance in each session. The exerted force was also averaged for every second and normalized in the same way (Fig. 1b).

Single-trial reconstruction of force

We used linear regression to reconstruct the changes in the force levels based on the changes of oxy-Hb concentrations in multiple channels (Fig. 2). The force y at time t is described as,

$$y(t) = b + \sum_C \sum_{u=-5}^{15} w_C(u) x_C(t+u) + \varepsilon(t), \tag{1}$$

where $x_C(t)$ is the oxy-Hb concentration of NIRS channel C at time t . The allocation of the channel index C is shown in Fig. 1c. The variable u denotes the time lag between the exerted force and oxy-Hb in seconds. Thus, the linear weight $w_C(u)$ is the weight parameter of

channel C with a lag of u seconds. The term b denotes the bias and $\varepsilon(t)$ is the residual error term that obeys a zero-mean Gaussian distribution. We defined lag u of -5 to 15 s as the calculation range in order to avoid concomitance of data from the previous and following epochs. The resulting time-lag dimension was 21. For simplicity, Eq. (1) can be rewritten when considering all of the data samples in matrix form,

$$\mathbf{Y} = \mathbf{W}\mathbf{X} + \mathbf{e}, \tag{2}$$

where $\mathbf{Y} = [y(1), y(2), \dots, y(T)]$ is a $1 \times T$ matrix representing the measured force, and T is the number of samples. \mathbf{X} is a $M \times T$ matrix, where M is the number of inputs, including the channels, time-lag dimensions, and bias term b (when using 24 channels and 21 time-lag dimensions, M is 505 ($24 \times 21 + 1$ (bias b))). The linear weight \mathbf{W} is a $1 \times M$ matrix and \mathbf{e} is a $1 \times T$ residual term. The reconstructed force $\hat{\mathbf{Y}}$ is given by,

$$\hat{\mathbf{Y}} = \hat{\mathbf{W}}\mathbf{X}, \tag{3}$$

where $\hat{\mathbf{W}}$ is the estimated linear weight ($1 \times M$ matrix).

Goodness-of-fit evaluation from cross-validation

To estimate the linear weight $\hat{\mathbf{W}}$ and evaluate the reconstruction performance independently, we divided the datasets of the 10 sessions into a training dataset of seven sessions and a test dataset of three sessions. We first determined $\hat{\mathbf{W}}$ from the training datasets by a sparse linear regression (see below). Next, in order to evaluate the generalization performance, i.e., how applicable the estimated weight was to unknown datasets, a goodness-of-fit (GOF) value was computed by applying $\hat{\mathbf{W}}$ to the test datasets, which were not used for the weight estimation.

$$\text{GOF} = 1 - \frac{\|\hat{\mathbf{Y}} - \mathbf{Y}\|^2}{\|\mathbf{Y} - \bar{\mathbf{Y}}\|^2}. \tag{4}$$

Here, $\|\cdot\|$ indicates the Euclidean norm, and $\bar{\mathbf{Y}}$ is the mean of \mathbf{Y} . If the GOF value is 1, the reconstruction is perfect and has no error, while a GOF value that is lower than zero indicates a poor reconstruction with large errors. In order to reduce the procedural bias due to the selection of particular training and test datasets, we performed cross-validation by repeating the above process for all of the combinations of the seven training and three test sessions (a total of 120 sets).

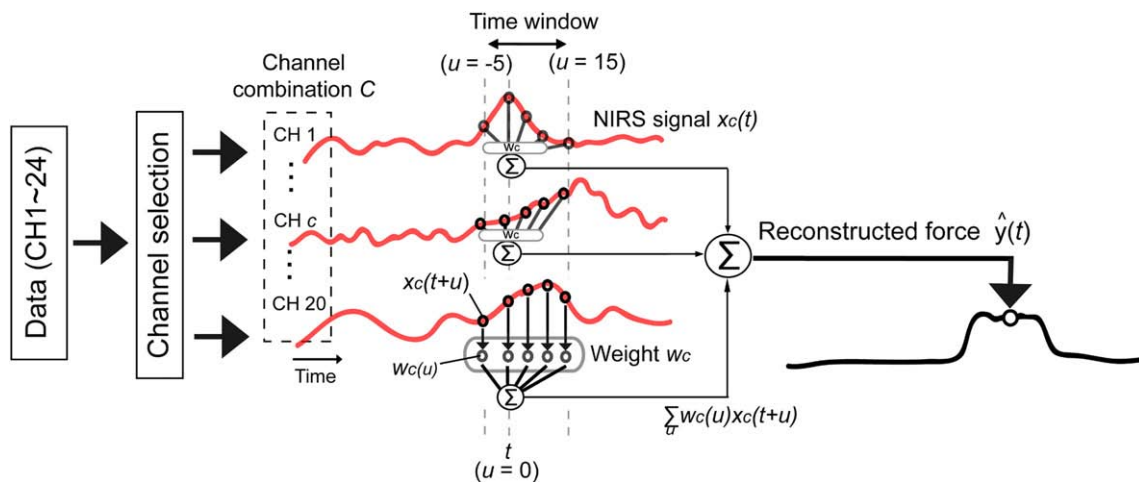


Fig. 2. Regression scheme with channel selection for a single-trial reconstruction. Linear regression was applied using a channel combination (C) determined by a channel selection method (the BRUTE-FORCE or the SPARSE method). For each selected channel, the NIRS signal (red line) of each time lag u , $x_C(t+u)$, was weighted by a linear weight $w_C(u)$ and summed up within the time window. Finally, these values were summed across channels ($\sum_{u=-5}^{15} w_C(u) x_C(t+u)$) to generate the reconstructed force signal \hat{y} (black line). The time window was set from time lag $u = -5$ to 15 .

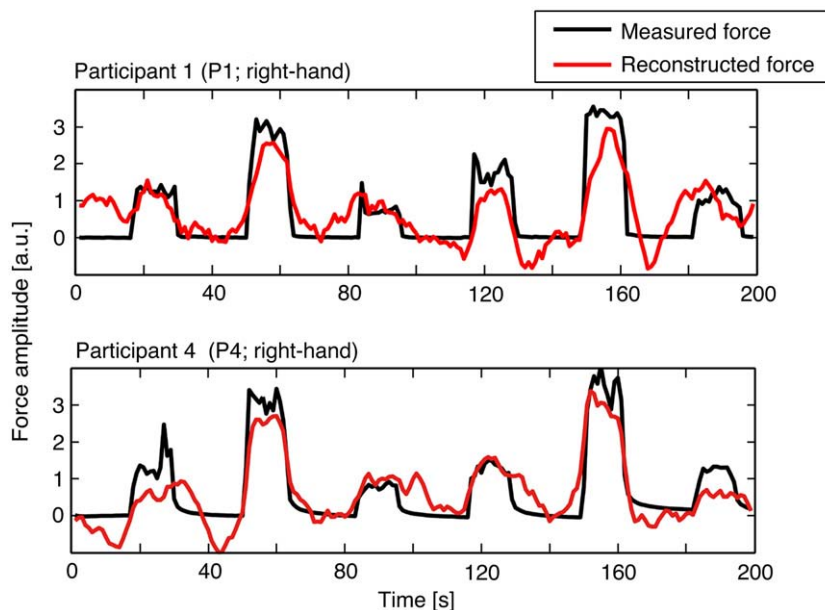


Fig. 3. Time-course of measured force and reconstructed force obtained from two participants. After the selection of the essential channels by the SPARSE method, the temporal changes in the measured force within a single trial (black line) from test datasets (sessions 8–10) were reconstructed (red line) from the oxy-Hb data using the linear weight obtained from the training datasets (sessions 1–7). The upper panel displays the right-hand data from session nine for a participant (P1; right-hand). The GOF value was 0.61. The lower panel displays the right-hand data from session nine for another participant (P4; right-hand). The GOF value was 0.73. The vertical and horizontal axes indicate the force amplitude (arbitrary unit; a.u.) and time (seconds).

Sparse linear regression (SPARSE)

We applied a sparse linear regression method, which have a generalization capability for unknown datasets due to their ability to remove irrelevant features (Sato, 2001; Ting et al., 2005, 2008; Ganesh et al., 2008). Here, we used a modified version of the sparse selection introduced in previous studies (Sato, 2001; Sato et al., 2004b; Toda et al., 2007; Ting et al., 2005, 2008), but differs from the sparse method for a previous fMRI study (Ganesh et al., 2008). We estimated the linear weight and the automatic relevance determination (ARD) parameters (Neal, 1996), which represent how the weight contributes to the reconstruction. Due to the analytical difficulty of estimating the parameters, we adopted the variational Bayesian method (Sato, 2001).

Thus, the present version is conceptually identical to those described above sparse method, with the exception that we considered ARD parameters for the spatial factor (i.e., channel) only, instead of all weight dimensions. Based on these ARD parameters, the SPARSE method identified only the channels that provided better generalization properties by pruning the ineffective channels for

reconstruction (setting the linear weight value equal to zero). This selection process provided a linear weight having a non-zero value only for a few channels, i.e., sparse representation.

The SPARSE method was compared with ordinary linear regression for all of the channels (ALL), as well as when using a brute-force combinatorial search (BRUTE-FORCE). More details of the SPARSE, ALL, and BRUTE-FORCE methods are described in the Appendix.

Results

Single-trial reconstruction performance of the sparse linear regression

By selecting the essential channels with the SPARSE method, the temporal changes in the measured force were well reconstructed from the oxy-Hb data. This was achieved by the estimation of the weight using the training dataset, and verified by application of the weight to the test dataset. The time-course for the measured force (black line) and for its reconstructed force (red line) in a representative session obtained from each of two representative participants can

Table 1
Reconstruction results from 120 cross-validation sets by the SPARSE method.

Participant	GOF value (mean (±SD))	Averaged number of channels selected (mean (±SD))	Frequency-based selected channel (rate [%])	GOF-based selected channel	Time lag provides the highest peak ($t_{highest}$ [s])
Right-hand					
P1	0.61 (±0.04)	3.9 (±0.9)	CH9# (100)	CH9#	5
P2	0.50 (±0.04)	3.6 (±1.0)	CH6# (100)	CH6#	4
P3	0.32 (±0.06)	4.5 (±0.9)	CH8 (97)	CH7#	14*
P4	0.68 (±0.04)	5.4 (±1.2)	CH9#, 3 (85)	CH9#	2
P5	0.37 (±0.06)	3.2 (±1.0)	CH3 (92)	CH3	0**
Left-hand					
P1	0.56 (±0.04)	3.3 (±0.9)	CH16# (92)	CH14	4
P2	0.39 (±0.09)	3.9 (±0.8)	CH19# (88)	CH22	5
P3	0.32 (±0.05)	3.8 (±0.7)	CH24 (98)	CH24	4

#These channels are located within approximately 30 mm of C3 or C4. Rate (%) equals the percentage of how often the channel was selected across 120 cross-validation sets. In participant 4 (P4), both CH3 and CH9 were equally frequently selected. As CH9 is closely located to C3, the data from CH9 was used for the across-participant analysis. *In participant 3 (P3), when we selected the channel (CH7) based on its GOF value (i.e., GOF-based selection), the time lag became 3 s. **In participant 5 (P5), the secondary, instead of the primary, peak of weight value in CH3 was observed at 5 s (see detail in the text).

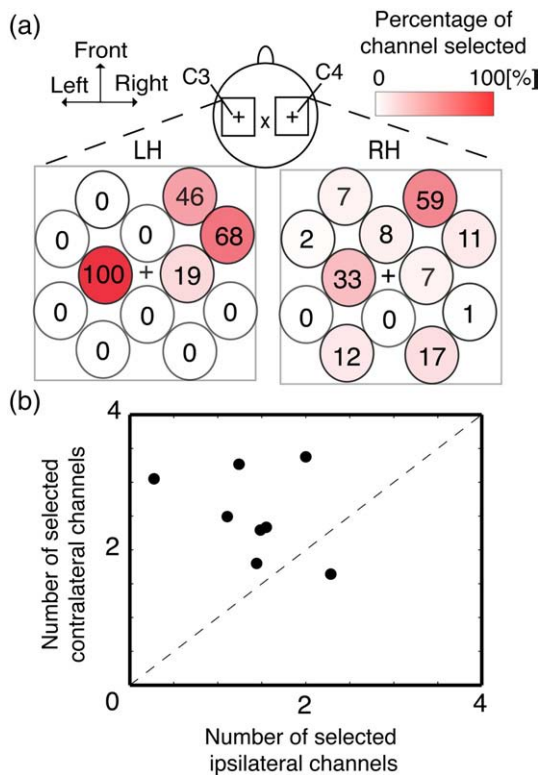


Fig. 4. Selection frequency of NIRS channels from all cross-validation sets. (a) Percentage of selected frequency in each channel over all 120 cross-validation sets in a representative participant (P1). Each circle represents a channel location that corresponds to that in Fig. 1c. The number in the circle, which is also graded by color, indicates the selection percentage when this participant performed with the right-hand. (b) The number of contralateral channels selected across the 120 cross-validation sets for each hand was plotted against that of the ipsilateral channels. The averaged number of selected channels across all cross-validation sets was calculated for each hemisphere of each hand. Each dot represents the data obtained from each hand. The horizontal axis (x-axis) indicates the number of the ipsilateral channels, and the vertical axis (y-axis) represents that of contralateral channels. In the majority of the tested hands, the contralateral channels were dominantly selected. The dashed line indicates $y=x$.

be seen in Fig. 3. These were examples of the best reconstruction in the present study, and their GOF values were 0.61 and 0.73, respectively.

When the GOF values were averaged across all test datasets (not from a particular session) for each hand, the average GOF values across eight hands ranged from 0.32 to 0.68 (mean \pm SD: 0.47 ± 0.14). We remark that these values were obtained when only a limited number (1 to 9) of channels were selected from all 24 channels. These GOF values were significantly greater than the baseline GOF (mean \pm SD: 0.04 ± 0.21 , Wilcoxon sign-rank test, $n=8$, $P<0.05$), which was computed by shuffling the channels of the test datasets 300-times. Randomly permuting the channels equals shuffling the spatial relation between the signals. In this way topographic information of the NIRS signals is eliminated in the baseline GOF. Table 1 summarizes the number of selected channels and GOF value for each hand.

Result of selected channels by cross-validation

Using the SPARSE method, we then validated the importance of the selected channels by performing a cross-validation throughout all 120 sets. Fig. 4a shows a representative example of selected frequency of each channel for right-hand sessions in a representative participant (P1). In these data, a total of 14 channels were selected in both hemispheres among all sets, while in individual set of cross-validation, a smaller number of channels (mean \pm SD: 3.9 ± 0.9) was

selected which was consistent across all hands in all participants (mean \pm SD: 4.0 ± 0.7). In this participant, the selected channels were predominantly located in the contralateral hemisphere. Indeed, when we evaluated the dominance of contralateral channels in all participants, the average number of selected contralateral channels across all of the cross-validation sets was significantly greater than that of the ipsilateral channels (Wilcoxon sign-rank test, $n=8$, $P<0.05$; see Fig. 4b).

In order to determine the most important channel, we adopted two selection criteria with respect to different aspects. In the first criteria we evaluated how often the same channel was selected over 120 cross-validation sets (frequency-based selection), while in the second criteria we searched for the channel having the highest GOF value among all selected channels (GOF-based selection). From the first criteria, we identified the most frequently selected channel among all cross-validation sets, while from the second criteria we determined the particular channel that most dominantly contributed to the reconstruction among all channels.

Table 1 summarized selected channels based on these two criteria in all hands (participants). In the frequency-based selection, the most frequently selected channels were located in the hemisphere contralateral to the performing hand, although their spatial location varied across hands. Likewise, in the GOF-based selection, the channels having the highest GOF values were located in the contralateral hemisphere in all hands. Thus, the frequency-based and the GOF-based selections provided identical channels or those channels located in a quite similar region (Table 1). Importantly, the

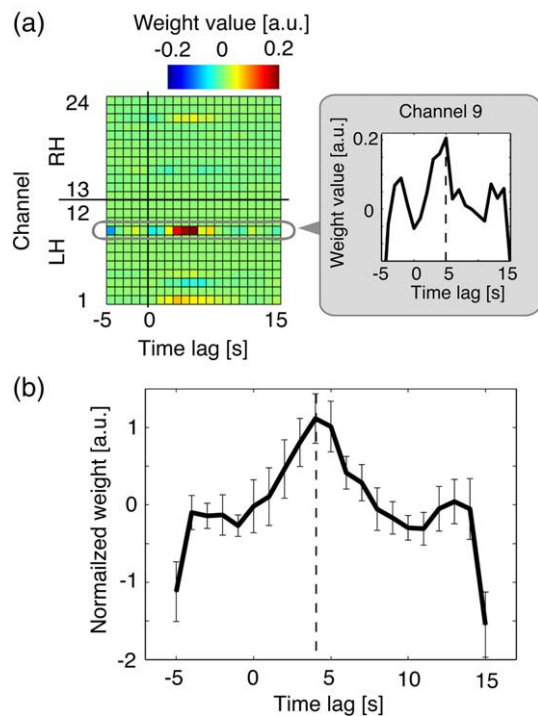


Fig. 5. Temporal profile of linear regression weight. (a) Linear regression weight for a representative participant (P1). The left panel summarizes the linear weight values for each channel (vertical axis) and its time lag (horizontal axis) when this participant performed with the right-hand. The linear weight is the average across those obtained from all 120 cross-validation sets. The weight values are indicated by graded colors, and the channels (1–12) belonging to the left hemisphere (LH) are displayed in the lower half of the panel. Green color is assigned to channels that have a weight value of 0 (i.e., channels not selected by the SPARSE method). The right panel shows the weight value changes for the most frequently selected channel (CH9). The dashed line indicates the time lag (5 s) that provided the highest weight value ($u_{highest}$). (b) The averaged normalized (z-scored) weight values across all of the hands for their most frequently selected channels. The weight values peaked at 4 s, as indicated by the dashed line. Error bars indicate standard deviations of weight values across all of the hands in each time lag.

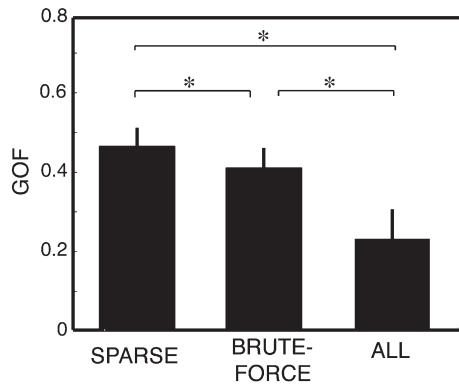


Fig. 6. Averaged GOF values for a test dataset across all of the hands in the three linear regression methods. The GOF value by the SPARSE method was significantly higher than those by the ALL and BRUTE-FORCE methods ($P < 0.01$). Error bars show standard errors.

contralateral channels were concentrated around C3 for right-hand movement and around C4 for left-hand movement in five out of eight hands in the frequency-based selection, and four out of eight hands in the GOF-based selection. Those channels can be assumed to be located close to the hand regions of the sensory-motor cortices.

Spatio-temporal linear weight

Fig. 5a (left panel) summarizes the average values of the linear weights across 120 cross-validation sets for each channel at each time lag u in the right-hand task of a representative participant (P1). The participant's most frequently selected channel was CH9 (see Fig. 5a right panel), the weight values of which changed according to time lag u , but which became largest when $u = 5$ s (u_{highest}). Similarly, the weights changed in accordance with the time lag u in all hands, and the time lags from the most frequently selected channels for all hands ranged from 0 to 14 s. Table 1 lists the time lag u_{highest} that gives the highest peak weight value for the most frequently selected channel for each hand. The peaks of the weights ranged from 2 to 5 s in six out of eight hands.

Next, we individually normalized the temporal profile of the weight value of the most frequently selected channel in each hand and then averaged across all hands (Fig. 5b). The averaged weight showed a positive value when the time lag u ranged from 0 to 8 s. The averaged weight value peaked at 4 s ($u_{\text{highest}} = 4$ s) after the time point of force exertion ($= 0$ s).

Comparison with other linear regression methods

To examine whether the SPARSE method was appropriate for the single-trial reconstruction of the finger-pinch force from NIRS signals, we compared the GOF values of the test dataset averaged across participants for the SPARSE, the BRUTE-FORCE, and the ALL methods (Fig. 6). The GOF values for these three methods were significantly different (Friedman test, $n = 8$, $P < 0.05$), with post-hoc analysis demonstrating that the GOF values for SPARSE was significantly higher than those obtained for ALL and BRUTE-FORCE (Wilcoxon signed-rank test, $n = 8$, $P < 0.01$), while those for BRUTE-FORCE were significantly higher than for ALL (Wilcoxon signed-rank test, $n = 8$, $P < 0.01$). In addition, the average number of channels across participants selected by SPARSE (range: 3.2 to 5.4; mean \pm SD: 4.0 ± 0.7 ; see Table 1) was significantly lower than that identified by BRUTE-FORCE (range: 6.0 to 9.4; mean \pm SD: 8.1 ± 1.1 ; Wilcoxon signed-rank test, $n = 8$, $P < 0.01$), indicating that SPARSE may produce a significantly higher GOF value while selecting a smaller number of channels when compared with BRUTE-FORCE.

Discussion

In the present study, we showed that the temporal changes in multiple finger-pinch force levels, including at resting state (force level 0), can be reconstructed from human sensory-motor cortical activation as measured by NIRS (oxy-Hb), thus advancing the current level of NIRS application, i.e., a binary classification of a sensory-motor event, to the level of linear reconstruction of a continuous event.

Methodological considerations

The reconstruction performance evaluated by the GOF values indicated the suitability of the present SPARSE method in handling NIRS oxy-Hb concentration data. As expected, the SPARSE and BRUTE-FORCE methods were superior to the ALL method, which may be the result of the channel selection process decreasing the possibility of over-fitting the oxy-Hb signals to the force data. It is generally accepted that over-fitting easily occurs when the number of samples is relatively small in comparison to the size of the estimated parameter dimension. This may have been the case in the present study when using ALL method. The size of the estimated linear weight dimension ($= 505$) may still have been too large when considering the number of samples, i.e., the training datasets ($199 \times 7 = 1393$ samples). In contrast, by selecting the essential channels with SPARSE and/or BRUTE-FORCE, we reduced the size of the estimated linear weight dimension (mean \pm SD: 83 ± 15 , 170 ± 23 , respectively) while the number of samples remains the same.

Over-fitting can also be observed by examining the difference in the GOF values between the training and test datasets. If over-fitting of training data occurs then the GOF value should become drastically smaller in the test datasets compared with the training datasets. Indeed, the reduction in the GOF value from the training datasets to the test datasets ($[\text{GOF in the training}] - [\text{GOF in the test}]$) was significantly greater in ALL (mean \pm SD: 0.54 ± 0.17) compared with SPARSE (0.11 ± 0.03) and BRUTE-FORCE (0.25 ± 0.06) (Wilcoxon signed-rank test, $n = 8$, $P < 0.01$, respectively). Thus, even though the NIRS parameter dimension was relatively small compared with other neuroimaging techniques such as fMRI, ALL had the problem of over-fitting, which was improved by using SPARSE and BRUTE-FORCE.

When we compared the two channel selection methods, SPARSE was superior to BRUTE-FORCE in terms of the GOF value and its computational cost. The total number of possible combinations in an exhaustive search was approximately sixteen million, which was too large for a best channel combination search. Even when we used the BRUTE-FORCE method, which efficiently searches for the best channel combination from a limited number of combination sets, the computational cost was greater than that for SPARSE. Indeed, SPARSE required a tenth of the computational time required by BRUTE-FORCE in the present study. In support of the view that SPARSE has an advantage for generalization, previous studies demonstrated the validity of sparse feature selection when muscular activity was reconstructed from unit recording data (Ting et al., 2005, 2008) and fMRI activation (Ganesh et al., 2008), as well as when various types of visual stimuli were decoded from fMRI activation (Yamashita et al., 2008). It is important to note, however, that SPARSE has a limitation in that we may have excluded some important channels (i.e., over-pruning) (Ganesh et al., 2008; Yamashita et al., 2008). Of course, increasing the number of collected data and improving the measurement accuracy may avoid over-pruning, and thereby improve the GOF value. Nevertheless, as far as the spatial location of selected channels is biologically plausible (see below), we believe that channel selection, such as with the SPARSE method, is useful to effectively select NIRS channels that reflect task-relevant brain activation while excluding those having false correlations with tasks containing background physiological signals.

Physiological plausibility of NIRS data

Using the present SPARSE method we found that the most frequently selected channels (i.e., the most important channels for reconstruction) were located in the hemisphere contralateral to the performing hand, particularly around C3 in the left hemisphere and C4 in the right hemisphere for five out of eight performing hands. Many event-related brain potential (ERP) studies have shown that brain activity recorded from those sites accurately reflects neuronal activity related to hand/finger sensory-motor events (Ikeda et al., 1992). Thus, although the spatial resolution and recording modality differ among these neuroimaging techniques, the locations of the majority of the selected channels can be assumed to correspond to the hand/finger sections of the primary sensory-motor cortices in the present study.

In order to confirm the importance of sensory-motor channels for force reconstruction, we conducted a preliminary experiment (not laid out in this study), where NIRS signals from the prefrontal regions (12 channels, the center of NIRS holder was located in the center point of a triangle formed by Fz, Fp1, and Fp2) and from the contralateral sensory-motor regions (12 channels, centered on C3 or C4) were measured simultaneously. One participant performed the same task as in the present study. Both right and left hands were tested. By applying exactly the same reconstruction approach using the SPARSE method, the channels most frequently selected by cross-validation were located indeed on the contralateral sensory-motor region around C3/C4 for both the right and left hand. The GOF values computed from the channels selected in the contralateral sensory-motor areas were significantly greater than that obtained from those in the prefrontal region. These data suggest a stronger contribution of the contralateral sensory-motor channels to the force reconstruction compared with other brain regions such as the prefrontal cortex that are less relevant to the task.

Although the contralateral primary sensory-motor cortex plays a primary role in the force generation task, other areas, including neighboring secondary sensory-motor areas, also play important roles in controlling and grading the hand/finger forces (Ehrsson et al., 2000; Dettmers et al., 1995, 1996; Cramer et al., 2002; Dai et al., 2001). Indeed, in the present study, the channels contributing to the force reconstruction were not only located in the contralateral primary sensory-motor cortex, but also in other neighboring cortical regions, including the pre-motor region. In particular, for two of the participants the best channels for the reconstruction (i.e., the most frequently selected channels) were selected from the neighboring regions in the contralateral hemisphere. Potentially, this may relate to individual differences in the relative location of the NIRS optodes to their cortices, a variability of channel sensitivity, or a strategic difference in controlling the force.

The averaged time lag that provided the highest weight values across participants (averaged u_{highest}) was approximately four seconds after the time point the force was to be reconstructed (Fig. 5). However, when we examined u_{highest} individually across all hands, the values ranged from 2 to 5 s in six out of eight hands, while the other two hands showed out-of-range values. When we selected the channel based on its GOF value (i.e., GOF-based selection) for one of those two hands (P3 right hand), the value peaked at 3 s, while for the other hand (P5 right hand) the secondary peak for the weight value in the channel (CH 3) selected both by the frequency- and the GOF-based selections was observed at 5 s after the time to be reconstructed. Thus, taken together, these data suggest that the primary peaks in the majority of tested hands, and the secondary peak of one hand, was in the range of the hemodynamic delay of the BOLD signal (several seconds after movement onset; Aguirre et al., 1998; Miezin et al., 2000; Handwerker et al., 2004). Indeed, fMRI–NIRS simultaneous measurement suggests that the oxy-Hb measured by NIRS reaches its peak at around 3 to 6 s after movement onset, which closely equals the hemodynamic delay of the BOLD signal measured

by fMRI (Huppert et al., 2006). This suggests that we indeed reconstructed the finger-pinch forces based on the NIRS signals (oxy-Hb) that reflected the sensory-motor cortical activation related to the force generation.

Single-trial reconstruction from multi-channel NIRS data

We consider that the reconstruction/prediction approach has an advantage in terms of extracting cortical activation from NIRS. Many NIRS studies have used the technique of averaging event-related NIRS data across trials and sessions to identify task-specific activation individually for each channel. Our approach conceptually distinguishes itself from that method, and was designed to identify the cortical activation essentially related to a task in a trial-based manner from multiple-channel data. In general, the NIRS signal likely contains background physiological signals including cardiac pulsations, respiration, and blood pressure variations (Obrig et al., 2000; Boas et al., 2004). In simultaneous measurements of these systemic signals and NIRS (Leung et al., 2003; Tachtsidis et al., 2008a,b), the changes of the systemic signals accompanied by the task were correlated with NIRS activation in brain areas which are unlikely related to a task (e.g., prefrontal area in the motor task). Under these measurement conditions, the conventional averaging technique may identify activation reflecting highly reproducible background physiological changes coinciding with a task as a task-related activation reflecting its brain computation. In addition, as optical permeability varies over the scalp, due to local differences in bone thickness for instance, the absolute amplitude of cortical activation does not necessarily completely reflect a purely task-related brain process.

In contrast, for our reconstruction/prediction approach using the SPARSE method, only channels whose signals essentially contributed to the force reconstruction may be selected, without any bias by the experimenter. Although those selected channels could incidentally become identical to those having larger amplitudes of activation, the level of activation at a single channel is not the main criterion and larger amplitude is not a prerequisite. Furthermore, principal component analysis (Boas et al., 2004; Zhang et al., 2005) and independent component analysis (Kohno et al., 2007) are also suitable for extracting components of brain signals. However, as these methods are not capable of examining the task-relevance of the components, then the reconstruction approach would be also applicable to those methods for essentially identifying task-relevant brain activation from NIRS data.

The results from the present study suggest that the linear regression method is generally valid for the reconstruction/prediction of continuous force changes over time, at least within the current range of generated force (Cramer et al., 2002), which is attributed to the following two reasons. First, both increasing as well as decreasing phases of force changes can be traced continuously by linear regression, which allowed us to reconstruct the generated forces regardless of their magnitudes. This is advantageous compared with binary classification methods. Second, due to its simplicity, linear regression was commonly used in previous studies where motor output was successfully reconstructed from neuronal activity (Carmena et al., 2003; Morrow and Miller, 2003; Koike et al., 2006; Townsend et al., 2006; Ting et al., 2005, 2008; Ganesh et al., 2008). In the future, once the measurement of a fast optical signal is established (Wolf et al., 2002), then quick reconstruction within a few hundred milliseconds will be available for NIRS applications using the quantitative feedback of brain activities (Ward et al., 2007; Birbaumer and Cohen, 2007) by taking advantage of the linear regression method for time-series data.

Conclusion

We demonstrated the potential for reconstructing temporal changes of multiple finger-pinch force levels, including resting state,

from human sensory-motor cortical activation measured by NIRS, and showed that the sparse linear regression was the most suitable method for single-trial reconstruction. As the best reconstruction was achieved when using the contralateral sensory-motor activation and when incorporating hemodynamic delay for majority of hands, the NIRS (oxy-Hb) channels that contribute to the regression likely include the information that reflects physiological changes in the cortices related to the neuronal processing for force generation with the hand/fingers. To our knowledge, this is the first NIRS study to demonstrate that the continuous levels of external loads (forces) can be reconstructed from their corresponding internal loads (activation) in restricted regions of the human brain. Thus, sparse linear regression may be applicable to the reconstruction of externally measurable loads from human brain activity in a wide range of tasks.

Acknowledgments

This research was supported by the National Institute of Information and Communications Technology (NICT) and the SCOPE, Ministry of Internal Affairs and Communications. We thank Y. Fujiwara, N. Hagura, K. Shibata, Y. Shimizu, and H. Tanaka for helpful comments and manuscript editing. We also thank anonymous reviewers for valuable suggestions.

Appendix A. Linear regression methods (ALL and BRUTE-FORCE)

A.1 Ordinary linear regression with all channels (ALL)

As a benchmark method, we employed common least square linear regression using all NIRS channels. We refer to this procedure as the ALL method. This is the simplest regression method since no selection of channels has to be conducted. The weight $\hat{\mathbf{W}}$ for the linear regression to reconstruct force \mathbf{Y} from NIRS signals \mathbf{X} is estimated as,

$$\hat{\mathbf{W}} = \mathbf{Y}\mathbf{X}^T(\mathbf{X}\mathbf{X}^T)^{-1}, \quad (5)$$

where superscript T is the transpose operator. We recall that in the ALL method, the number of input M is 505 (24 channels \times 21 time-lags + bias), and thus $\hat{\mathbf{W}}_{\text{ALL}}$ has 505 dimensions ($= 24 \times 21 + 1$).

A.2 Ordinary linear regression with brute-force channel selection (BRUTE-FORCE)

In the BRUTE-FORCE method channels were pre-selected before applying regression. As a search for all of the possible channel-combinations (approximately sixteen million sets) is exhausting and requires huge computational cost, the BRUTE-FORCE method takes the more efficient approach of searching for the best combination. In detail, we exclude some channel-combinations from candidates, and select a limited number of channel-combinations that provide better GOF values as the candidates for the next search step. The best channel combination is determined among the selected candidate channel-combinations by again looking at the GOF values. A parameter n_{CH} indicates the number of channels in one combination. The linear weight was estimated from training datasets as follows:

1. $n_{\text{CH}} = 1$: Calculate the GOF value for each channel as a 1-channel combination.
2. Repeat from $n_{\text{CH}} = 2-24$.
 - 2.1 Select the top 20 ($n_{\text{CH}} - 1$) channel-combinations as candidates based on the GOF value computed at 2.3 in the previous step (e.g., in $n_{\text{CH}} = 2$, we select 20 one-channel combinations (CH^{1st}-CH^{20th}) and exclude remaining four sets (CH^{21th}-CH^{24th})). Here, CH^{*i*th} denotes the channel combination with the *i*th highest GOF value.
 - 2.2 Define the candidate n_{CH} -channel-combinations. New possible candidate combinations are constructed from each of the ($n_{\text{CH}} - 1$)

channel combinations selected in 2.1 by adding one of the remaining channels to it. For example, in $n_{\text{CH}} = 2$, we construct combinations of one of the candidate 20 channel combinations (e.g., CH1) and one of the remaining 23 channels (from CH2-CH24). This results in 270 pair of 2-channel combinations, i.e., [CH1, CH2], [CH1, CH3], ... [CH20, CH24]).

- 2.3 Calculate the GOF value for each selected n_{CH} -channel-combinations. The ordinary least square method (Eq. (5)) is used to determine the linear weight. The GOF value is estimated a leave-one-out cross-validation using the training datasets.
3. After evaluating the step 2 for $n_{\text{CH}} = 1-24$, we determine the channel combination with the highest GOF value as the optimal channel-combination set, $\mathbf{C}_{\text{BRUTE}}$.
4. Estimate linear weight for $\mathbf{C}_{\text{BRUTE}}$. The linear weight $\hat{\mathbf{W}}_{\text{BRUTE}}$ the dimension of which equals the channel dimension of $\mathbf{C}_{\text{BRUTE}}$ is estimated from \mathbf{X} and \mathbf{Y} in all of the training datasets using Eq. (5).

The above procedure describes the BRUTE-FORCE channel selection with a forward search (by adding channels). We confirmed that the optimal set found by the forward search was consistent with that of a backward search (by eliminating channels).

Appendix B. Regression with sparse channel selection (SPARSE)

A brief explanation of the present sparse channel selection is given below (see previous literature for more details (Sato, 2001; Sato et al., 2004b; Ting et al., 2005, 2008)).

In a probabilistic model of linear regression (Eq. (2)), the likelihood function can be described as a probabilistic model,

$$P(\mathbf{Y}|\mathbf{X}, \mathbf{W}, \sigma) = \frac{1}{(2\pi)^{T/2}} \sigma^{T/2} \exp \left[-\frac{1}{2} \sigma^2 (\|\mathbf{Y} - \mathbf{W}\mathbf{X}\|^2) \right], \quad (6)$$

where T is the number of samples and \mathbf{X} is a $M \times T$ matrix. M is the number of inputs, which includes the channels ($N_{\text{CH}} = 24$) and time-lag dimensions ($N_{\text{L}} = 21$), i.e., $M = N_{\text{CH}} \times N_{\text{L}}$ ($24 \times 21 = 504$). For simplicity, we consider the case in which \mathbf{X} and \mathbf{Y} are normalized to have a zero-mean (i.e., the term b in Eq. (1) is set to 0).

Here, we introduce automatic relevance determination (ARD) priors (Neal, 1996). As ARD priors, we assume that the precision parameter α and the noise variance σ . In the general case, a precision parameter α would be introduced for each of M inputs (see previous literature). However, in the present study we intended to select channels while keeping the temporal dimension constant. Thus, we assume that α is embedded for each channel i , but not for time-lag dimension j , i.e., $\alpha_{ij} = \alpha_i$ for all j . We assume a normal distribution prior of \mathbf{W} , and the hierarchical ARD priors α and σ are described as,

$$P_0(\mathbf{W}|\alpha) = \prod_{j=1}^{N_{\text{L}}} \prod_{i=1}^{N_{\text{CH}}} \frac{1}{(2\pi)^{1/2}} \alpha_i^{1/2} \exp \left[-\frac{1}{2} \alpha_i w_{ij}^2 \right],$$

$$P_0(\alpha) = \prod_{i=1}^{N_{\text{CH}}} \alpha_i^{-1} \quad (7)$$

$$P_0(\sigma) = \sigma^{-1}.$$

The subscript 0 indicates fixed parameters. α is the N_{CH} vector. \mathbf{w} is the component of \mathbf{W} . Note that the time-lag index $j=1$ here, corresponds to $u = -5$ in the text.

Next, we consider the weight parameter \mathbf{W} given the training datasets (\mathbf{X} and \mathbf{Y}). The weight can be estimated by evaluating the following posterior joint probability of \mathbf{W} ,

$$P(\mathbf{W}, \alpha, \sigma | \mathbf{X}, \mathbf{Y}) = \frac{P(\mathbf{Y}, \mathbf{W}, \alpha, \sigma | \mathbf{X})}{P(\mathbf{Y}|\mathbf{X})} = \frac{P(\mathbf{Y}|\mathbf{X}, \mathbf{W}, \sigma) P_0(\mathbf{W}|\alpha) P_0(\alpha) P_0(\sigma)}{P(\mathbf{Y}|\mathbf{X})}, \quad (8)$$

$$P(\mathbf{Y}|\mathbf{X}) = \int d\mathbf{W} d\alpha d\sigma P(\mathbf{Y}, \mathbf{W}, \alpha, \sigma | \mathbf{X}).$$

Since analytical solution is difficult to find, we applied the variational Bayesian method (Attias, 1999; Sato, 2001) to obtain the posterior distribution $P(\mathbf{W}, \boldsymbol{\alpha}, \sigma | \mathbf{X}, \mathbf{Y})$. In the variational Bayesian approximation, $P(\mathbf{W}, \boldsymbol{\alpha}, \sigma | \mathbf{X}, \mathbf{Y})$ is calculated by approximating a trial distribution $Q(\mathbf{W}, \boldsymbol{\alpha}, \sigma)$. This approximation can be performed by the maximization of the variational free energy $F(Q)$,

$$F(Q) = \int d\mathbf{W}d\boldsymbol{\alpha}d\sigma Q(\mathbf{W}, \boldsymbol{\alpha}, \sigma) \log \frac{P(\mathbf{Y}, \mathbf{W}, \boldsymbol{\alpha}, \sigma | \mathbf{X})}{Q(\mathbf{W}, \boldsymbol{\alpha}, \sigma)}. \quad (9)$$

Thus, estimating the weight \mathbf{W} is equivalent to finding the parameters that maximize $F(Q)$.

To obtain the maximum $F(Q)$, we assume that the distributions $Q(\mathbf{W}, \boldsymbol{\alpha}, \sigma)$ can be factorized into distributions which restricts the solution space,

$$Q(\mathbf{W}, \boldsymbol{\alpha}, \sigma) = Q_{\mathbf{W}}(\mathbf{W})Q_{\boldsymbol{\alpha}}(\boldsymbol{\alpha}, \sigma). \quad (10)$$

By means of this factorization, the maximum $F(Q)$ is obtained by two iterative steps. One is referred to as W -step, and maximizes $F(Q)$ with respect to $Q_{\mathbf{W}}$. The other, α -step maximizes $F(Q)$ with respect to $Q_{\boldsymbol{\alpha}}$. These two steps are alternatively repeated until the free energy $F(Q)$ converges.

<W-step>

In the W -step, we maximize $F(Q)$ with respect to $Q_{\mathbf{W}}$ while $Q_{\boldsymbol{\alpha}}$ is fixed. We can determine the update equations for the linear weight \mathbf{W} and regularized input covariance $\Sigma_{\mathbf{W}}$ as,

$$\begin{aligned} \bar{\mathbf{W}} &= \bar{\sigma}(\mathbf{Y}\mathbf{X}^T) \cdot \Sigma_{\mathbf{W}}^{-1}, \\ \Sigma_{\mathbf{W}} &= \bar{\sigma}(\mathbf{X}\mathbf{X}^T) + \bar{\mathbf{A}}, \end{aligned} \quad (11)$$

where $\bar{\sigma}$ are the expectation values estimated in the α -step, and $\bar{\mathbf{A}}$ is a diagonal matrix whose $(N_{\text{CH}}(j-1) + i)$ th diagonal elements for all j are the i th component of the precision parameter $\boldsymbol{\alpha}$ (i.e., $\bar{A}_{N_{\text{CH}}(j-1) + i, N_{\text{CH}}(j-1) + i} = \bar{\alpha}_i$).

< α -step>

Likewise, $F(Q)$ is maximized with respect to $Q_{\boldsymbol{\alpha}}$ while $Q_{\mathbf{W}}$ is fixed. The precision vector $\boldsymbol{\alpha}$, and noise variance σ are updated as follows,

$$\begin{aligned} \bar{\sigma}^{-1} &= \frac{1}{T} (\|\mathbf{Y} - \bar{\mathbf{W}}\mathbf{X}\|^2) + \text{Tr}(\Sigma_{\mathbf{W}}^{-1}\mathbf{X}\mathbf{X}^T), \\ \bar{\alpha}_i^{-1} &= \frac{1}{2} \sum_{j=1}^{N_i} \left(\bar{w}_{N_{\text{CH}}(j-1) + i}^2 + (\Sigma_{\mathbf{W}}^{-1})_{N_{\text{CH}}(j-1) + i, N_{\text{CH}}(j-1) + i} \right), \end{aligned} \quad (12)$$

where Tr indicates the trace, and $(\Sigma_{\mathbf{W}}^{-1})_k$ is the k th diagonal component of the inverse covariance matrix $\Sigma_{\mathbf{W}}^{-1}$.

After the convergence of the free energy $F(Q)$ is achieved, the weight of irrelevant input dimensions are pruned (the corresponding weight is eliminated). We define the linear weight $\bar{\mathbf{W}}$ after convergence as $\hat{\mathbf{W}}_{\text{SPARSE}}$. Using $\hat{\mathbf{W}}_{\text{SPARSE}}$, the GOF was evaluated for the test datasets.

We remark, that the sparse linear regression laid out above, differs from regression that recently applied in an fMRI study (Ganesh et al., 2008). In the latter a Bayesian version of Least Absolute Shrinkage and Selection Operator (LASSO) was used, where an open parameter that determines complexity (i.e., the number of the fMRI voxels) is initially estimated by manual tuning or cross-validation. In the method above (SPARSE), such parameter is determined automatically.

References

Aguirre, G.K., Zarahn, E., D'Esposito, M., 1998. The variability of human BOLD hemodynamic responses. *NeuroImage* 8 (4), 360–369.

Attias, H., 1999. Inferring parameters and structure of latent variable models by variational Bayes. *Proc. 15th Conference on Uncertainty in Artificial Intelligence*, Morgan-Kaufman, pp. 21–30.

Birbaumer, N., Cohen, L.G., 2007. Brain-computer interfaces: communication and restoration of movement in paralysis. *J. Physiol.* 579, 621–636.

Boas, D.A., Dale, A.M., Franceschini, M.A., 2004. Diffuse optical imaging of brain activation: approaches to optimizing image sensitivity, resolution, and accuracy. *NeuroImage* 23 (Suppl 1), S275–S288.

Carmena, J.M., Lebedev, M.A., Crist, R.E., O'Doherty, J.E., Santucci, D.M., Dimitrov, D.F., Patil, P.G., Henriquez, C.S., Nicolelis, M.A., 2003. Learning to control a brain-machine interface for reaching and grasping by primates. *PLoS Biol.* 1, e42.

Cheney, P.D., Fetz, E.E., 1980. Functional classes of primate corticomotoneuronal cells and their relation to active force. *J. Neurophysiol.* 44, 773–791.

Coyle, S., Ward, T., Markham, C., McDarby, G., 2004. On the suitability of near-infrared (NIR) systems for next-generation brain-computer interfaces. *Physiol. Meas.* 25, 815–822.

Coyle, S.M., Ward, T.E., Markham, C.M., 2007. Brain-computer interface using a simplified functional near-infrared spectroscopy system. *J. Neural Eng.* 4, 219–226.

Cramer, S.C., Weisskoff, R.M., Schaechter, J.D., Nelles, G., Foley, M., Finklestein, S.P., Rosen, B.R., 2002. Motor cortex activation is related to force of squeezing. *Hum. Brain Mapp.* 16, 197–205.

Dai, T.H., Liu, J.Z., Sahgal, V., Brown, R.W., Yue, G.H., 2001. Relationship between muscle output and functional MRI-measured brain activation. *Exp. Brain Res.* 140, 290–300.

Dettmers, C., Fink, G.R., Lemon, R.N., Stephan, K.M., Passingham, R.E., Silbersweig, D., Holmes, A., Ridding, M.C., Brooks, D.J., Frackowiak, R.S., 1995. Relation between cerebral activity and force in the motor areas of the human brain. *J. Neurophysiol.* 74, 802–815.

Dettmers, C., Connelly, A., Steohan, K.M., Turner, R., Friston, K.J., Frackowiak, R.S., Gadian, D.G., 1996. Quantitative comparison of functional magnetic resonance imaging with positron emission tomography using a force-related paradigm. *NeuroImage* 4 (3), 201–209.

Ehrsson, H.H., Fagergren, A., Jonsson, T., Westking, G., Johansson, R.S., Forssberg, H., 2000. Cortical activity in precision- versus power-grip tasks: an fMRI study. *J. Neurophysiol.* 83 (1), 528–536.

Evarts, E.V., 1968. Relation of pyramidal tract activity to force exerted during voluntary movement. *J. Neurophysiol.* 31, 14–27.

Ganesh, G., Burdet, E., Haruno, M., Kawato, M., 2008. Sparse linear regression for reconstructing muscle activity from human cortical fMRI. *NeuroImage* 42 (4), 1463–1472.

Handwerker, D.A., Ollinger, J.M., D'Esposito, M., 2004. Variation of BOLD hemodynamic responses across subjects and brain regions and their effects on statistical analyses. *NeuroImage* 21 (4), 1639–1651.

Hatakenaka, M., Miyai, I., Mihara, M., Sakoda, S., Kubota, K., 2007. Frontal regions involved in learning of motor skill—a functional NIRS study. *NeuroImage* 34 (1), 109–116.

Hoshi, Y., 2003. Functional near-infrared optical imaging: utility and limitations in human brain mapping. *Psychophysiology* 40, 511–520.

Hoshi, Y., Kobayashi, N., Tamura, M., 2001. Interpretation of near-infrared spectroscopy signals: a study with a newly developed perfused rat brain model. *J. Appl. Physiol.* 90, 1657–1662.

Huppert, T.J., Hoge, R.D., Diamond, S.G., Franceschini, M.A., Boas, D.A., 2006. A temporal comparison of BOLD, ASL, and NIRS hemodynamic responses to motor stimuli in adult humans. *NeuroImage* 29 (2), 368–382.

Ikeda, A., Lüders, H.O., Burgess, R.C., Shibasaki, H., 1992. Movement-related potentials recorded from supplementary motor area and primary motor area. Role of supplementary motor area in voluntary movements. *Brain* 15 (4), 1017–1043.

Koike, Y., Hirose, H., Sakurai, Y., Iijima, T., 2006. Prediction of arm trajectory from a small number of neuron activities in the primary motor cortex. *Neurosci. Res.* 55, 146–153.

Koizumi, H., Yamashita, Y., Maki, A., Yamamoto, T., Ito, Y., 1999. Higher-order brain function analysis by trans-cranial dynamic near-infrared spectroscopy imaging. *J. Biomed. Opt.* 4 (4), 403–413.

Koizumi, H., Yamamoto, T., Maki, A., Yamashita, Y., Sato, H., Kawaguchi, H., Ichikawa, N., 2003. Optical topography: practical problems and new applications. *Appl. Opt.* 42, 3054–3062.

Kohno, S., Miyai, I., Seiyama, A., Oda, I., Ishikawa, A., Tsuneishi, S., Amita, T., Shimizu, K., 2007. Removal of the skin blood flow artifact in functional near-infrared spectroscopic imaging data through independent component analysis. *J. Biomed. Opt.* 12 (6), 062111.

Leung, T.S., Elwell, C.E., Henty, J., Delpy, D.T., 2003. Simultaneous measurement of cerebral tissue oxygenation over the adult frontal and motor cortex during rest and functional activation. *Adv. Exp. Med. Biol.* 510, 385–389.

Maki, A., Yamashita, Y., Ito, Y., Watanabe, E., Mayanagi, Y., Koizumi, H., 1995. Spatial and temporal analysis of human motor activity using noninvasive NIR topography. *Med. Phys.* 22, 1997–2005.

Miezin, F.M., Maccotta, L., Ollinger, J.M., Petersen, S.E., Buckner, R.L., 2000. Characterizing the hemodynamic response: effects of presentation rate, sampling procedure, and the possibility of ordering brain activity based on relative timing. *NeuroImage* 11 (6), 735–759.

Miyai, I., Tanabe, H.C., Sase, I., Eda, H., Oda, I., Konishi, I., Tsunazawa, Y., Suzuki, T., Yanagida, T., Kubota, K., 2001. Cortical mapping of gait in humans: a near-infrared spectroscopic topography study. *NeuroImage* 14 (5), 1186–1192.

Morrow, M.M., Miller, L.E., 2003. Prediction of muscle activity by populations of sequentially recorded primary motor cortex neurons. *J. Neurophysiol.* 89, 2279–2288.

- Neal, R.M., 1996. Bayesian learning for neural networks. *Lect. Notes Stat.* 118 Springer.
- Obrig, H., Hirth, C., Junge-Hülsing, J.G., Döge, C., Wolf, T., Dirnagl, U., Villringer, A., 1996. Cerebral oxygenation changes in response to motor stimulation. *J. Appl. Physiol.* 81 (3), 1174–1183.
- Obrig, H., Neufang, M., Wenzel, R., Kohl, M., Steinbrink, J., Einhäupl, K., Villringer, A., 2000. Spontaneous low frequency oscillations of cerebral hemodynamics and metabolism in human adults. *NeuroImage* 12 (6), 623–639.
- Obrig, H., Villringer, A., 2003. Beyond the visible—imaging the human brain with light. *J. Cereb. Blood Flow Metab.* 23, 1–18.
- Sato, M.A., 2001. Online model selection based on the variational Bayes. *Neural Comp.* 13, 1649–1681.
- Sato, H., Kiguchi, M., Kawaguchi, F., Maki, A., 2004a. Practicality of wavelength selection to improve signal-to-noise ratio in near-infrared spectroscopy. *NeuroImage* 21 (4), 1554–1562.
- Sato, M.A., Yoshioka, T., Kajihara, S., Toyama, K., Goda, N., Doya, K., Kawato, M., 2004b. Hierarchical Bayesian estimation for MEG inverse problem. *NeuroImage* 23 (3), 806–826.
- Sitaram, R., Zhang, H., Guan, C., Thulasidas, M., Hoshi, Y., Ishikawa, A., Shimizu, K., Birbaumer, N., 2007. Temporal classification of multichannel near-infrared spectroscopy signals of motor imagery for developing a brain-computer interface. *NeuroImage* 34 (4), 1416–1427.
- Tachtsidis, I., Leung, T.S., Tisdall, M.M., Devendra, P., Smith, M., Delpy, D.T., Elwell, C.E., 2008a. Investigation of frontal cortex, motor cortex and systemic haemodynamic changes during anagram solving. *Adv. Exp. Med. Biol.* 614, 21–28.
- Tachtsidis, I., Leung, T.S., Devoto, L., Delpy, D.T., Elwell, C.E., 2008b. Measurement of frontal lobe functional activation and related systemic effects: a near-infrared spectroscopy investigation. *Adv. Exp. Med. Biol.* 614, 397–403.
- Thickbroom, G.W., Phillips, B.A., Morris, I., Byrnes, M.L., Sacco, P., Mastaglia, F.L., 1998. Differences in functional magnetic resonance imaging of sensorimotor cortex during static and dynamic finger flexion. *Exp. Brain Res.* 126, 431–438.
- Ting, J.A., D'Souza, A., Yamamoto, K., Yoshioka, T., Hoffman, D.S., Kakei, S., Lauren, S., Kalaska, J.F., Kawato, M., Strick, P.L., Schaal, S., 2005. Predicting EMG data from M1 neurons with Variational Bayesian least squares. *Proceedings of Advances in Neural Information Processing Systems 18 (NIPS2005)*. MIT press, Cambridge, MA.
- Ting, J.A., D'Souza, A., Yamamoto, K., Yoshioka, T., Hoffman, D.S., Kakei, S., Lauren, S., Kalaska, J.F., Kawato, M., Strick, P.L., Schaal, S., 2008. Variational Bayesian least squares: an application to brain-machine interface data. *Neural Networks* 21 (8), 1112–1131.
- Toda, A., Imamizu, H., Sato, M., Wada, Y., Kawato, M., 2007. Reconstruction of temporal movement from single-trial non-invasive brain activity: a hierarchical Bayesian method. *The 14th International Conference on Neural Information Processing (ICONIP2007)*.
- Townsend, B.R., Paninski, L., Lemon, R.N., 2006. Linear encoding of muscle activity in primary motor cortex and cerebellum. *J. Neurophysiol.* 96 (5), 2578–2592.
- Villringer, A., Chance, B., 1997. Non-invasive optical spectroscopy and imaging of human brain function. *Trends Neurosci.* 20 (10), 435–442.
- Ward, T.E., Soraghan, C.J., Matthews, F., Markham, C., 2007. A concept for extending the applicability of constraint-induced movement therapy through motor cortex activity feedback—using a neural prosthesis. *Comput. Intell. Neurosci.* Article ID 51363, 9 p.
- Watanabe, E., Yamashita, Y., Maki, A., Ito, Y., Koizumi, H., 1996. Non-invasive functional mapping with multi-channel near infra-red spectroscopic topography in humans. *Neurosci. Lett.* 205 (1), 41–44.
- Wolf, M., Wolf, U., Choi, J.H., Gupta, R., Safonova, L.P., Paunescu, L.A., Michalos, A., Gratton, E., 2002. Functional frequency-domain near-infrared spectroscopy detects fast neuronal signal in the motor cortex. *NeuroImage* 17 (4), 1868–1875.
- Yamashita, O., Sato, M.A., Yoshioka, T., Tong, F., Kamitani, Y., 2008. Sparse estimation automatically selects voxels relevant for the decoding of fMRI activity patterns. *NeuroImage* 42 (4), 1414–1429.
- Zhang, Y., Brooks, D.H., Franceschini, M.A., Boas, D.A., 2005. Eigenvector-based spatial filtering for reduction of physiological interference in diffuse optical imaging. *J. Biomed. Opt.* 10 (1), 11014.